DLS and AFM Studies on the Cluster Evolution of Organically Modified Silica Gels Catalyzed by a Super Strong Acid

Yusuke Takata,[†] Tomohisa Norisuye,*[,†] Satoshi Hirayama,[†] Tsuyoshi Takemori,[†] Qui Tran-Cong-Miyata,[†] and Shigeki Nomura[‡]

Department of Macromolecular Science and Engineering, Graduate School of Science & Technology, Kyoto Institute of Technology Matsugasaki, Sakyo-ku, Kyoto 606-8585, Japan, and R&D Center, Sekisui Chemical Co., Ltd., 32 Wadai, Tsukuba-shi, Ibaraki 300-4292, Japan

Received November 7, 2006; Revised Manuscript Received March 14, 2007

ABSTRACT: Time evolution of cross-linking clusters prepared by the sol−gel method was investigated by dynamic light scattering (DLS) and atomic force microscopy (AFM). The samples were prepared by the sol−gel synthesis of 1,8-bis(triethoxysilyl)octane (Tes-Oct) in the presence of phosphotungstic acid (PWA) as a super strong acid. The reaction batches were quenched at various reaction times, followed by dilution with a large amount of the solvent. DLS and AFM techniques simultaneously revealed that there exists a maximum cluster size, R_h and r_{AFM}, respectively, for a specific PWA concentration. The information on the clusters density, $\rho_{cluster} = (r_{AFM}/R_h)^3$, generated during the reaction process was obtained by systematically comparing the DLS data obtained in the swollen state to the AFM data measured in the shrunken state of the cross-linked clusters. It was found that not only the cluster size but also $\rho_{cluster}$ exhibited a maximum for [PWA]/[Tes-Oct] = 0.10 near the gel point of the Tes-Oct clusters. Since PWA is not only a super strong acid as a catalyst for the sol−gel synthesis but is also a proton conductor, the resulting materials can be utilized as a fuel-cell membrane. The ac impedance measurements revealed that the proton conductivity also exhibited a similar maximum at this specific PWA concentration, revealing the optimum condition for design of conducting membrane.

Introduction

Cross-linking has attracted considerable attention in the field of polymer chemistry and engineering because of the potential for compensation to limited properties of linear polymers. Besides the significant improvement of thermal and mechanical properties of polymer materials, cross-linking offers entirely new functionalities via supporting or binding ligands, semiconductors, catalysts, and so on. Among a wide variety of advanced materials, sol−gel-derived polymer hybrids containing a proton conductor are one of the promising candidates for fuel cell applications due to the effective support of conductors in the matrix and the high thermal stability of the materials.[1−4]

In our previous work, we have demonstrated that organic−inorganic polymer hybrids containing phosphotungstic acid (PWA), a heteropolyacid, exhibited fairly good performance of the proton conductivity.[5] Note that PWA has two important roles, i.e., a super strong acid for the sol−gel reaction and a proton conductor suitable for a fuel cell application.[6] Unlike a large number of conducting materials, which exhibits an ionic channel of the conductive phase,[7−9] we have observed a domain structure developed by the effective growth and coarsening of the domains where constituting particles would contain a sufficient amount of the conductor and be mutually connected without segregation of PWA or leaking PWA.[4]

Before discussing how super strong acids give rise to the network structure in sol−gel processing, let us explain the basis of the sol−gel reaction. In general, the sol−gel process can be classified into two different routes.[10,11] One is particle growth in a basic condition, where dissociated hydroxyl ions promote a nucleophilic reaction. The larger particles with the size up to several hundred nanometers can be generated as long as the growing particles are stabilized by the repulsive surface interaction. On the other hand, a network structure with less branching points is formed when the reaction is carried out in an acidic condition. Since most of the acidic conditions are not too far from the isoelectric point of alkoxysilanes, typically around pH 2, the effect of the catalyst is not so pronounced in the reaction. Thus, the reaction in the acidic condition results in chain extension consisting of small primary particles, which

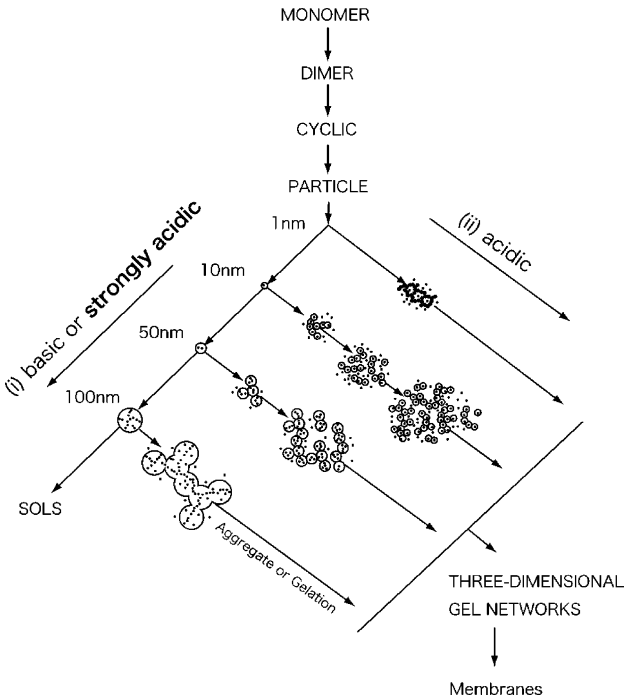

Figure 1. Schematic representation of the evolution of clusters and subsequent aggregates and/or network formation in the sol−gel process. PWA was drawn by the gray dots.

* To whom correspondence should be addressed.
[†] Kyoto Institute of Technology.
[‡] Sekisui Chemical Co., Ltd.

10.1021/ma062570a CCC: $37.00
Published on Web 04/14/2007

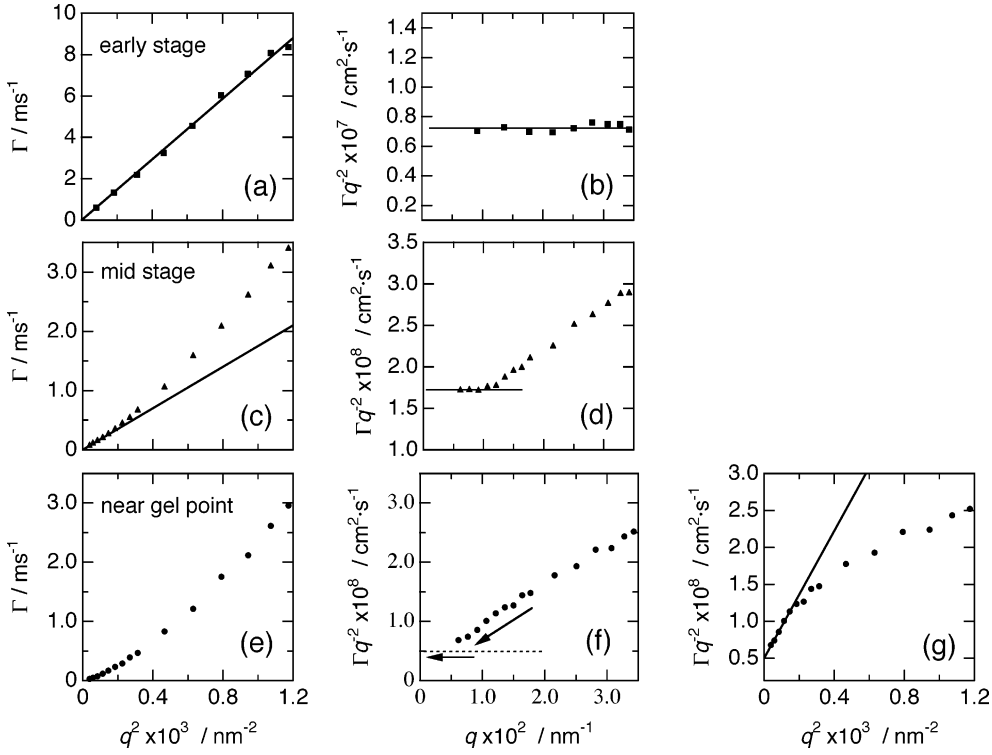

Figure 2. Examples of the initial decay rate analysis for various stages of the reaction.

significantly differs from the basic system. The schematic representation of the pH dependence of the sol−gel process, which is an extended picture of the Iler's model,[12] is illustrated in Figure 1.

It is expected that the reaction under basic conditions is a suitable route to design better proton conductive membranes from a sol−gel process since the larger amount of the conductor can be incorporated into large element particles rather than leaking through voids or the domains boundary. PWA should be localized near the reaction front of a sol−gel precursor, resulting in PWA with hydrated water being well trapped inside the silica particle since its hydrated water is indispensable for the sol−gel reaction. This could prevent serious leaking of the proton conductors existing near the surface of or between aggregated particles. However, it is not allowed to expose the conductors in a basic solution because PWA is disintegrated at the higher pH so that the approach has been limited to acidic catalyses. In our previous work, we observed that the reaction process of silica gels with a heteropolyacid, a super strong acid, was significantly different from typical reactions of conventional acidic systems.[4] For example, in-situ dynamic light scattering (DLS) revealed that (1) evolution of the intensities and relaxation time quite resembled those of basic conditions and (2) the fast mode fraction to the total intensity, A_f, was fairly high throughout the reaction. From these facts, it was expected that the element particles are highly stabilized by the presence of charges and are allowed to grow beyond the limitation of the conventional acidic catalysis approach. This opened a possibility to utilize sol−gel derived membranes containing a heteropolyacid as proton conductive membranes for fuel cell applications.

In order to understand the relationship between the proton conductivity and the microscopic structure of such materials, it is interesting to investigate the formation process of the desired structure. The objectives of this study are (i) to find a route to maximize the cluster size and (ii) to obtain information on the development of the clusters throughout the reaction. Although the previous work provided us some guidelines to understand process of unique cluster evolution process, it remained unclear whether the gelation originated from the growth of a single cluster due to strong acid catalyst or from the aggregation of the developing clusters. To clarify this mechanism, first, the concentration and angular dependence of DLS measurements were performed after quenching the sample at various reaction times. This enables us to estimate the cluster size in the swollen state. Subsequently, the diluted clusters are casted on a silicon wafer, followed by direct observation of the cluster size and its distribution in the shrunken state by atomic force microscopy (AFM). Combining the forementioned information further allows us to obtain the density information on the clusters for the better understanding of the reaction process and the structure of the clusters.

Experimental Section

Samples. Sol−gel precursor, 1,8-bis(triethoxysilyl)octane (Tes-Oct; Gelest), $(OC_2H_5)_3-Si-(CH_2)_8-Si-(OC_2H_5)_3$, was purified twice by reduced pressure distillation. Phosphotungstic acid (PWA; Aldrich), $H_3PW_{12}O_{40}$, and isopropanol (IPA; Wako Chemical, Japan) were used as received. Note that PWA plays a role not only as a proton conductor in the PWA dispersed membrane but also as a super strong acid catalyst for the reaction. The concentration of PWA was adjusted to several molar ratios of PWA to Tes-Oct, $r_{PWA} = 0.050$, 0.100, 0.150, and 0.200. For comparison, the acid-catalyzed Tes-Oct samples in the absence of PWA ($r_{PWA} = 0$) were prepared using 1 N hydrochloric acid (HCl; Wako Chemical, Japan). The concentration of Tes-Oct, c_{TES}, was kept at 18.67 wt %. The reaction batch was prepared by adding a mixture (PWA + water + IPA) into a (Tes-Oct + IPA) mixture to initiate the reaction. After vigorous stirring, the solution was filtered through a Teflon membrane of the pore size 0.25 μm and poured into a purified test tube. The reaction was quenched by dilution with a large amount of solvents at various reaction times for the DLS measurements. DLS experiments were performed at $c_{TES} = 1.87$ wt %, below which the concentration dependence of the diffusion coefficient was negligible. The stock solutions were further diluted, followed by casting on a silicon wafer in a vacuum chamber to obtain samples for the AFM measurements.

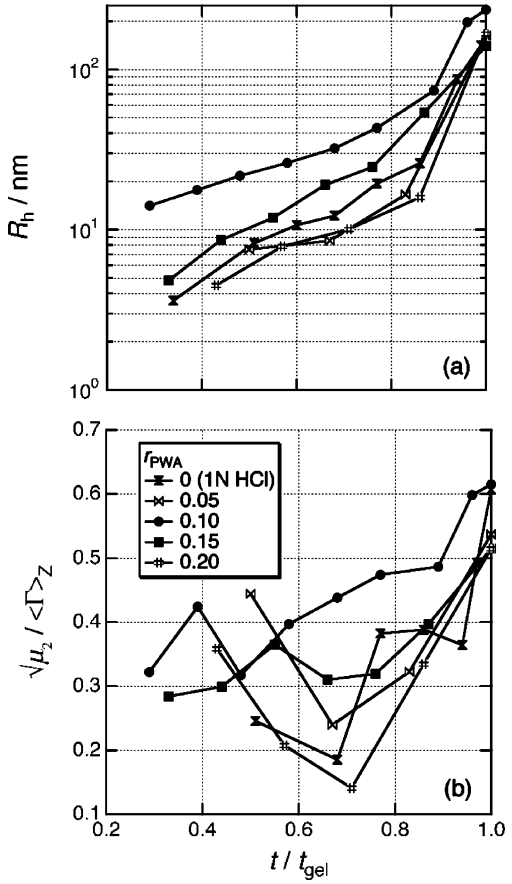

Figure 3. Time evolution of (a) R_h and (b) normalized standard deviation of Γ obtained for different PWA concentrations.

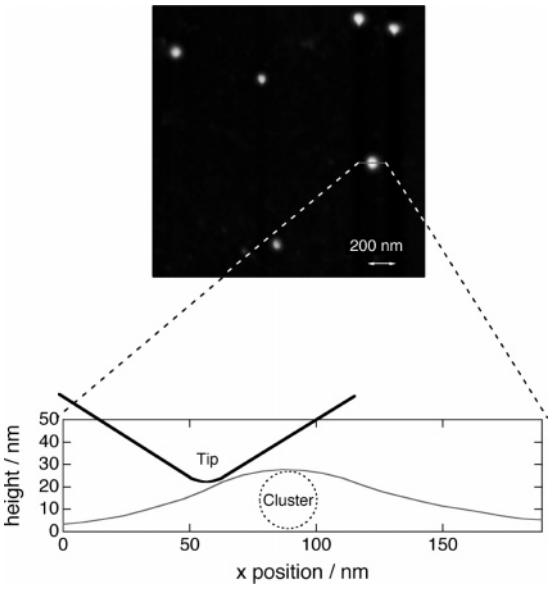

Figure 4. (a) AFM topography of the Tes-Oct/PWA clusters for $r_{PWA} = 0.10$ at $t/t_{gel} = 0.7$. (b) Schematic representation of a line profile observed by AFM.

Samples Characterization. Dynamic Light Scattering (DLS). DLS measurements were carried out on a DLS7000 linear photon correlator system (Otsuka Electronics Co., Japan) equipped with an Ar laser (NEC; 75 mW). The sampling time was set to an optimum value to obtain a fully decaying intensity correlation function (ICF), which was typically 4 μs with 1024 channels. The correlation functions were recorded in the angular range 20°−150°, with an angular step depending on the particle size. The experimental was carried out in a thermostat bath regulated at 30 ± 0.1 °C.

Atomic Force Microscopy (AFM). AFM was operated in the tapping mode using a Digital Instruments Multimode AFM, controlled by a Nanoscope IIIa scanning probe microscope controller with an extender module. Commercially available silicon tip with a spring constant of 30−40 N/m and single beam cantilevers of 125 μm long was used at resonance frequencies ranging from 310 to 340 kHz. Several topographies were obtained using tapping mode with a scan rate of 1 Hz in ambient atmosphere at room temperature. Before performing the AFM measurements for the cross-linked clusters, a pure silicon wafer and a standard polystyrene latex with a known diameter were scanned respectively to ensure the level of background and to calibrate AFM. Then the AFM images for the Tes-Oct clusters were collected by scanning different regions of the sample until the average and standard deviations of the cluster distribution become invariant.

Results and Discussion

The initial slope of the semilogarithmic plot of intensity correlation functions, $g^{(2)}(t)$, provides the *z*-average decay rate, $\langle\Gamma\rangle_z$, expressed by

$$\langle\Gamma\rangle_z = -\frac{1}{2}\lim_{t\to 0}\left[\frac{\mathrm{d}\ln\{g^{(2)}(t)-1\}}{\mathrm{d}t}\right] \tag{1}$$

In general, $\langle\Gamma\rangle_z$ depends on the concentration, c, and the magnitude of the scattering vector, q, expressed by[13,14]

$$\langle\Gamma\rangle_z = Dq^2(1 + k_D c + ...)(1 + f_D q^2 R_h^2) \tag{2}$$

where D, k_D, and f_D are respectively the *z*-averaged translational diffusion constant, second virial coefficient for DLS, and a constant for the q dependence of DLS. When the hydrodynamic radius, R_h, is much smaller than the inverse of q in a dilute limit, eq 2 is reduced to

$$\langle\Gamma\rangle_z = Dq^2 = \frac{k_B T q^2}{6\pi\eta R_h} \tag{3}$$

where k_BT and η are the Boltzmann energy and solvent viscosity, respectively. If samples are polydisperse, a distribution of Γ must be considered. By expanding the logarithm of ICF in a power series in t, one may obtain $\langle\Gamma\rangle_z$ by[15]

$$\frac{1}{2}\ln\{g^{(2)}(t)-1\} = -\langle\Gamma\rangle_z t + \frac{\mu_2}{2!}t^2 + ... \tag{4}$$

where $\sqrt{\mu_2}$ is the standard deviation of Γ.

In the initial stage of reactions, $\langle\Gamma\rangle_z$ is proportional to q^2 as demonstrated in Figure 2a. This corresponds to the invariance of D over a wide range of wave vectors, suggesting that DLS measurement at a fixed angle could give the particle sizes equivalent to those obtained by the angular dependent measurements (Figure 2b). However, as the reaction proceeds, the particle size becomes larger, resulting in the interference of an internal (or rotational) mode to the translational mode. This additional effect is responsible for the nonlinear behavior of $\langle\Gamma\rangle_z$ vs q^2 plot (Figure 2c) or the appearance of the nonconstant behavior of $\langle\Gamma\rangle_z/q^2$ at high q (Figure 2d). Nevertheless, it is still possible to obtain the plausible particle size from the plateau region of the plot provided that one could have sufficient data points in the small q region. When the reaction proceeds further and the solution eventually approaches the gelation threshold, neither the initial slope of $\langle\Gamma\rangle_z$ vs q^2 plot (Figure 2e) nor the plateau at low-q region (Figure 2f) can be exactly determined. Alternatively, $\langle\Gamma\rangle_z/q^2$ is plotted vs q^2 to obtain the intercept D and the initial slope $f_D R_h^2$, as shown in Figure 2g. It should be

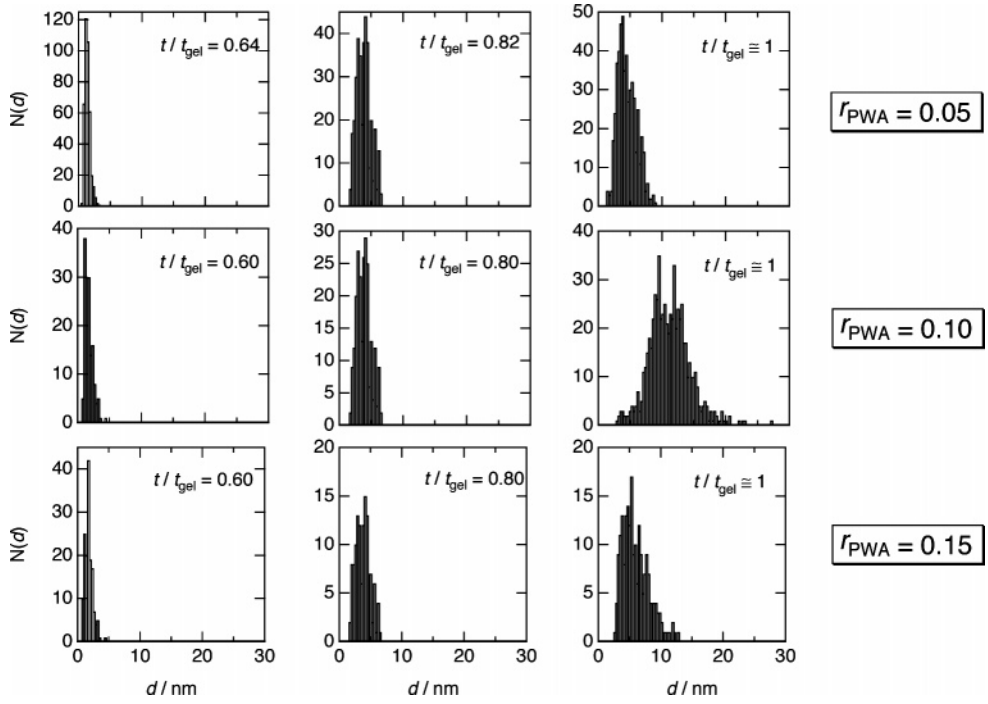

Figure 5. Cluster size distribution of the Tes-Oct clusters quenched at the different stages of the reaction obtained for various PWA concentrations.

noted that the cluster size obtained for the Tes-Oct/PWA system remained at ca. 100 nm, although the molar mass is generally considered to diverge upon gelation as predicted by the classical theory.[16] Similar behavior was observed in the previous study for systems with fixed water concentration.[4] Furthermore, even if the cluster size remains finite, the correlation function observed in situ (without dilution of the sample) exhibited a power law when the reaction approached the gel point. Note that the present correlation functions do not exhibit a bimodal relaxation time distribution since the samples are fairly in dilute condition.

Figure 3a shows the time course of R_h obtained by this procedure for the Tes-Oct/PWA system with different PWA concentrations. As seen from the figure, R_h increased with the reaction time for all of the PWA concentrations. However, R_h for $r_{PWA} = 0.10$ exhibited the largest cluster sizes throughout the reaction process, which was similar to the previous finding that R_h exhibited maxima for the same PWA concentration. While the amount of water was fixed to $[H_2O]/[\text{Tes-Oct}] = 0.5$ in the previous study, the water contents of the present system increased together with the PWA concentration since PWA containing certain number of hydrated water was used without drying treatment. In general, water plays an important role in the sol−gel reaction. However, it was found that the unique maximum of R_h in the PWA concentration dependence appeared irrespective of the water contents or dehydration treatment of PWA, suggesting PWA plays a more important role rather than reaction water in the present sol−gel system.

Figure 3b shows the time course of the normalized standard deviation of Γ obtained by the cumulant analysis. Although this is not directly ascribed to the cluster size but to the diffusion coefficient, it suggests that the cluster size distribution becomes more or less broad as the reaction goes on. Particularly, the normalized standard deviation for $r_{PWA} = 0.10$ was the largest, which was also similar to the time evolution of R_h. In order to disclose the characteristic of the reaction and the structure of the clusters, it is of great interest to gain information on the average size but also to visualize clusters with their distribution.

It is well-known that AFM topography suffers from overestimation of the domain size in the horizontal direction,[17,18] leading to the broadening of domains traced by a tip with a finite volume (Figure 4). In order to obtain the reliable particle size from the lateral direction in the topography, a deconvolution operation is required.[19−21] However, this requires great knowledge about the tip shape. Therefore, in this study, the height information was employed[22] in order to evaluate the cluster diameter as exhibited in Figure 4. The figure shows several Tes-Oct/PWA clusters casted on a silicon wafer in the swollen state. The height of the particles was extracted from an AFM image with the scanning size of 2000 nm after removal of the background. It should be noted that AFM is no longer nondestructive if there is a deformation effect by probe-tip pressure. In order to ensure correct imaging, we investigated the stability of AFM height evaluated upon repetitive scanning of the clusters at the same location. As a result, we obtained the same cluster size irrespective of the scanning times within 1% error over different scanning times. If there were the deformation effects in our system, the obtained size would systematically decrease. Therefore, we believe the deformation effect due to probe-tip pressure is not a serious problem in our case unless the clusters have already been in the deformed state after the first trial.

The data obtained by AFM in this way were processed by the following method of image analysis. First, the AFM image was smoothed to identify particles with various sizes. As the target particles were successfully found, their height was extracted, followed by construction of the histogram after subtraction of the background. Figure 5 shows the histogram of the cluster diameter, d, for $r_{PWA} = 0.05$, 0.10, and 0.15 at different reaction times. The evolution of the Tes-Oct/PWA clusters was clearly confirmed by the fact that the peak value of the cluster size shifted toward the larger value and the histogram became broadened as the reaction proceeded.

Figure 6a shows the time evolution of the average cluster radius, r_{AFM}, of the Tes-Oct/PWA clusters. The maximal cluster size was found for $r_{PWA} = 0.10$, indicating that this particular

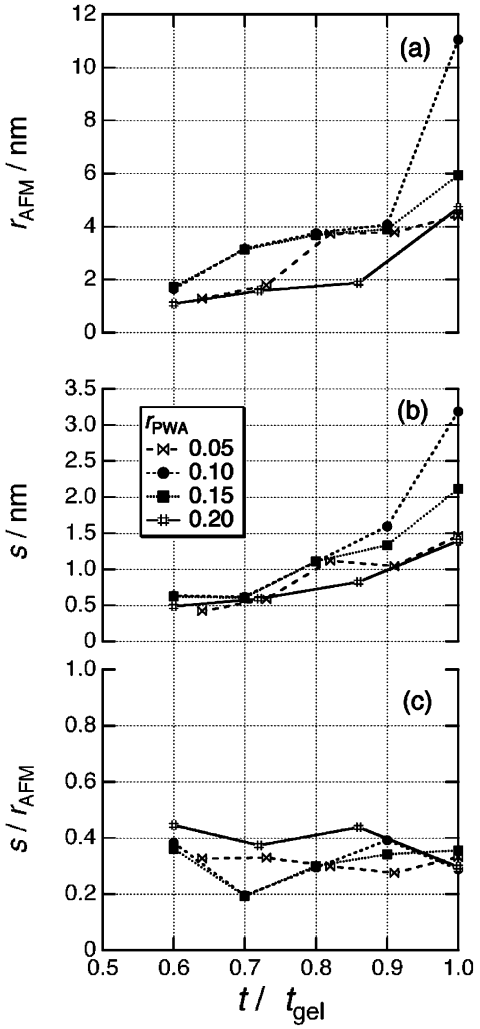

Figure 6. Time course of (a) r_{AFM}, (b) the standard deviation, s, and (c) the normalized standard deviation, s/r_{AFM}, of the cluster size with different r_{PWA}s.

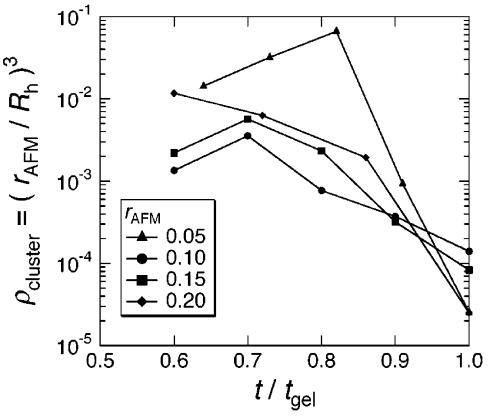

Figure 7. Time course of $\rho_{cluster}$ for different r_{PWA}s.

concentration is the most effective for the cluster evolution regardless of amount of hydrated water. The standard deviation, s, was depicted in Figure 6b. As the reaction proceeds, s becomes larger. This can be explained as follows: As gelation goes on, the molecular weight and its distribution generally become larger. Even if the polymerization is controlled by some sort of "living" techniques, the resultant cluster distribution becomes broader because of the fact that individual cluster can take either larger or smaller clusters.[23,24] Particularly s was has a largest value for $r_{PWA} = 0.10$. On the contrary to the results of DLS, the normalized standard deviations of AFM cluster size were smaller than those obtained by DLS and rather constant irrespective of both the PWA concentration and reaction time, as shown in Figure 6c.

In order to disclose the unique cluster evolution of $r_{PWA} = 0.10$ as observed in DLS and AFM experiment, it is of great interest to evaluate the ratio of the cluster sizes obtained by DLS and AFM since R_h was observed in the swollen state and r_{AFM} was obtained after drying treatment. Figure 7 shows the time course of a deswelling degree of these clusters defined by

$$\rho_{cluster} \equiv \left(\frac{r_{AFM}}{R_h}\right)^3 \tag{5}$$

for different PWA concentrations.

Interestingly, $\rho_{cluster}$ was the highest for $r_{PWA} = 0.05$ in the early stage of the reaction, followed by the reduction as the gel point is approached. Although the cluster size itself obtained for $r_{PWA} = 0.05$ is small, the reaction seems to proceed effectively with the limited amount of PWA as seen from the time course of $\rho_{cluster}$. However, $\rho_{cluster}$ dramatically decreased for $t/t_{gel} > 0.8$, suggesting the cluster aggregation occurred when PWA was exhausted by consumed in the late stage of the reaction. Since the sol−gel reaction requires water for hydrolysis of alkoxysilanes, which should be hydrated around PWA, it is considered that most of the PWAs will be trapped inside the clusters during the cluster growth process unless they are phase-separated or segregated. In other words, the PWA might loose its activity as a strong catalyst by entrapped inside the highly condensed clusters.

For $r_{PWA} = 0.10$, $\rho_{cluster}$ remained at the same order throughout the reaction, finally reaching the maximum among different r_{PWA}s. The smaller $\rho_{cluster}$ for $r_{PWA} = 0.10$ may be attributed to the larger R_h in the swollen state due to effective charge repulsion during the reaction. Since the larger amount of PWA was introduced for $r_{PWA} = 0.10$, the activity of PWA might persist until the late stage of the reaction and results in more gradual reduction of $\rho_{cluster}$ compared with the case $r_{PWA} = 0.05$. Although similar time evolution of $\rho_{cluster}$ was also found for $r_{PWA} = 0.15$, the cluster sizes observed by DLS and AFM themselves were not so large. Thus, we arrive at the conclusion that $r_{PWA} = 0.10$ may be the best system capable of incorporation of the largest amount of PWA into the clusters. When a gelation process was observed in-situ by DLS without dilution of the reacting sample, we noticed that the fraction of the first mode, A_f, was anomalously large for $r_{PWA} = 0.10$ unseen in conventional acidic systems. The unique behavior of the cluster size and the relative amplitude of the correlation function can be explained by the competition between (1) stabilization of the concentration fluctuations due to dissociation of the large anion of PWA and (2) promotion of phase separation upon further introduction of PWA.

While $\rho_{cluster}$ can be related to the density, the cross-linked clusters are bulky and rigid so that those will occupy the larger volume in the dry state than that expected from the absolute density. However, we believe that cluster size evaluated by AFM is the relevant parameter to explore the mechanism of the better proton conduction in a fuel cell application because a hybrid membrane is composed of such primary clusters. The better proton conductivity may be obtained if the clusters can highly swell upon water immersion, resulting in interconnection of domains with a large amount of water. Note that the density of the clusters can be alternatively determined by combination of M_w and R_h if the former is determined by static light scattering.

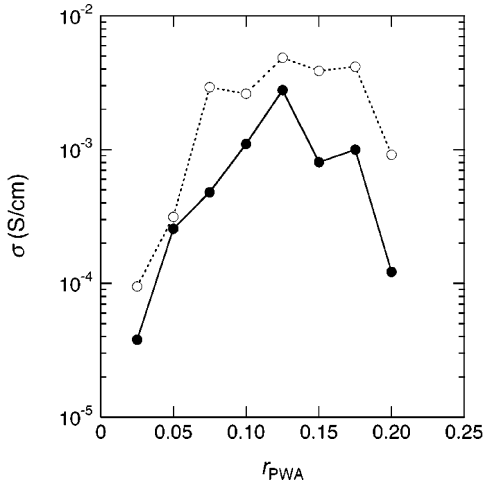

Figure 8. PWA concentration dependence of the proton conductivity, σ, for the Tes-Oct/PWA membranes with (solid circle) and without (open circle) drying treatment.

Finally, Figure 8 shows the PWA concentration dependence of the proton conductivity, σ, for a series of Tes-Oct/PWA membranes. The measurements were performed in a thermoregulator bath operated at 60 °C/95% RH. The membranes were prepared by mixing the stock solutions of Tes-Oct/IPA and PWA/IPA, followed by casting on a plastic Petri dish to evaporate the residual IPA. The open circles indicated that σ had a maximum at a specific PWA concentration ($r_{PWA} = 0.125$), reminiscent of the optimum reaction route found by DLS and AFM ($r_{PWA} = 0.10$). Although exactly matching the maximum location was not achieved, the DLS and AFM measurements have been carried out in order to investigate the structural evolution before the gelation threshold under the same sample concentration. This is significantly different from the case of the conductivity measurements in the membrane state where the membrane properties will be sensitively affected not only by cluster evolution but also by solvent evaporation and further solidification.

Conclusions

Both dynamic light scattering and atomic force microscopy measurements revealed that sol−gel-derived hybrids with a super strong acid exhibited optimum cluster evolution at particular acid concentration. In this study, 1,8-bis(triethoxysilyl)octane (Tes-Oct) and phosphotungstic acid (PWA) were respectively employed as a precursor and a super strong acid catalyst to prepare organic−inorganic hybrids. In the case of the hybrid network fabricated by a conventional acid catalyst, e.g., hydrochloric acid, the reactant becomes unstable when the cluster size approaches several nanometers, leading to a weakly branched aggregates/network structure. A similar behavior was found when the PWA concentration is relatively low ($r_{PWA} \sim 0.05$). As the PWA concentration increased ($r_{PWA} \sim 0.10$), the effect of PWA as a super strong acid was more pronounced. Namely, in spite of the fact that the reaction was carried out in an acid regime, the domain evolution was very similar to a base-catalyzed reaction due to effect of the large anion inherent in polyacid systems, resulting in the larger cluster formation. For $r_{PWA} > 0.15$, such a significant effect of PWA was screened out, and instead, the system became unstable to lead strong aggregation or macrophase separation. In this case, the particle growth again remained in several nanometers because of the instability. Since the clusters were respectively measured in the swollen and shrunken states for DLS and AFM, further analysis combining DLS and AFM data allowed one to obtain information on the developing of the clusters. The proton conductivity measurements for a series of Tes-Oct/PWA membranes were performed by using an ac impedance method. As a result, the conductivity also exhibited a maximum at a specific PWA concentration. Although the quantitative agreement on the optimum PWA concentration between the conductivity and cluster size has not yet achieved, the discrepancy could arise from the fact that the structural analysis was performed at the fixed concentration during gelation, while the conductivity measurement was carried out in the membrane state, which had various factors to determine the properties, such as aging accompanying solvent evaporation and domain growth beyond the gel point.

Acknowledgment. This work was supported by Grant-in-Aid No. 16750189 from the Ministry of Education, Science, Sports, Culture, and Technology.

References and Notes

(1) Tatsumisago, M.; Honjo, H.; Sakai, Y.; Minami, T. *Solid State Ionics* **1994**, *74*, 105.

(2) Lavrencic Stangar, U.; Groselj, N.; Orel, B.; Colomban, P. *Chem. Mater.* **2000**, *12*, 3745.

(3) Honma, I.; Nomura, S.; Nakajima, H. *J. Membr. Sci.* **2001**, *185*, 83.

(4) Aoki, Y.; Norisuye, T.; Tran-Cong-Miyata, Q.; Nomura, S.; Sugimoto, T. *Macromolecules* **2003**, *36*, 9935.

(5) Nakanishi, T.; Norisuye, T.; Sato, H.; Takemori, T.; Tran-Cong-Miyata, Q.; Nomura, S. *Macromolecules*, in press.

(6) Mohapatra, S. K.; Boyd, G. D.; Storz, F. G.; Wagner, S. *J. Electrochem. Soc.* **1979**, *126*, 805.

(7) Rollins, H. W.; Lin, F.; Johnson, J.; Ma, J.-J.; Liu, J.-T.; Tu, M.-H.; DesMarteau, D. D.; Sun, Y.-P. *Langmuir* **2000**, *16*, 8031.

(8) Won, J.; Park, H. H.; Kim, Y. J.; Choi, S. W.; Ha, H. Y.; Oh, I.-H.; Kim, H. S.; Kang, Y. S.; Ihn, K. J. *Macromolecules* **2003**, *36*, 3228.

(9) Lehmani, A.; Durand-Vidal, S.; Turq, P. *J. Appl. Polym. Sci.* **1998**, *68*, 503.

(10) Brinker, C. J.; Scherer, G. W. *Sol-Gel Science*; Academic Press: London, 1990.

(11) Yamane, M.; Inoue, S.; Yasumori, A. *J. Non-Cryst. Solids* **1984**, *63*, 13.

(12) Iler, R. K. *The Chemistry of Silica*; Wiley: New York, 1979.

(13) Brown, W.; Fundin, J. *Macromolecules* **1991**, *24*, 5171.

(14) Galinsky, G.; Burchard, W. *Macromolecules* **1995**, *28*, 2363.

(15) Koppel, D. E. *J. Chem. Phys.* **1972**, *57*, 4814.

(16) Stauffer, D. *Introduction to Percolation Theory*; Taylor & Francis: London, 1985.

(17) Paige, M. F.; Rainey, J. K.; Goh, M. C. *Micron* **2001**, *32*, 341.

(18) Leung, E. C. W.; Markiewicz, P.; Goh, M. C. *J. Vac. Sci. Technol. B* **1997**, *15*, 181.

(19) Tabet, M. F.; Urban, F. K., III *J. Vac. Sci. Technol. B* **1997**, *15*, 800.

(20) Markiewicz, P.; Goh, M. C. *Langmuir* **1994**, *10*, 5.

(21) Reiss, G.; Schneider, J.; Vancea, J.; Hoffmann, H. *Appl. Phys. Lett.* **1990**, *57*, 867.

(22) Xu, Z.; Ford, W. T. *Macromolecules* **2002**, *35*, 7662.

(23) Norisuye, T.; Takeda, M.; Shibayama, M. *Macromolecules* **1998**, *31*, 5316.

(24) Norisuye, T.; Morinaga, T.; Tran-Cong-Miyata, Q.; Goto, A.; Fukuda, T.; Shibayama, M. *Polymer* **2005**, *46*, 1982.

MA062570A